Load frequency control in Island micro-grid with electric vehicles and renewable energy sources using modified fractional order PID controller

Omokhafe James Tola[1], Ovis Daniel Irefu[2], James Garba Ambafi[1]
[1]Department of Electrical and Electronics Engineering, Federal University of Technology, Minna, Nigeria
[2]Department of Electrical Engineering, UNT College of Engineering, University of North Texas, Denton, United States

Article Info

ABSTRACT

This paper presents a modified fractional-order proportional-integral-differential (MFOPID) controller for load frequency control in an Island microgrid based on an electric vehicle (EV) and renewable energy source. It tackles the intermittent energy sources and the dynamic of the load change with reduced speed and the quality of response generated on the microgrid. The MFOPID controller gains are well turned using a metaheuristic grasshopper optimization algorithm (GOA) technique to determine its robustness and optimal system performance. The controller gains are evaluated with three different searching agent populations. The proposed MFOPID with GOA improved system performance frequency by 19.485 Hz compared to 14.1151 Hz of the benchmark model. It takes 6.9068 s of the proposed model to settle compared to 16.6796 s of FOPID.

Corresponding Author:

Omokhafe James Tola
Department of Electrical and Electronics Engineering, Federal University of Technology
P. M.B. 65, 920101, Minna, Niger, Nigeria
Email: ovisirefu@my.unt.edu

1.   INTRODUCTION

The development of vehicle-to-grid technology enables electric cars (EVs) to use various auxiliary services in a competitive electric market. EVs offer a chance to develop brand-new grid management services and products. If the agreements between the market participants are broken, EVs, a new type of distributed energy storage, can make up for the uncontracted power in the area [1]. Due to the quick advancement of vehicle-to-ride (V2R) technology, plug-in electric vehicles (PEVs) are one type of distributed energy storage projected to play a significant role in emergency reliability services. On the other side, EVs are becoming increasingly popular since they experience net cost savings and consume less gasoline and produce fewer greenhouse gases, which helps keep the environment clean [2]. The study [3], underlines the necessity of constructing a significant number of charging stations and facilities to handle the rising number of electric vehicles and the need for enhanced integration of renewable energy sources and more effective delivery of frequency regulation services. The researchers recommended future studies on the effects of electric vehicles on complicated power systems, such as microgrids that are isolated from a macro-grid and have a high penetration of renewable energy sources.

The expected trends in the automotive industry development are EVs, which are environmentally friendly and energy-saving cars [4]. This technology is a worthy choice for substantially reducing gasoline consumption emissions of greenhouse gases and precursors. A charging EV is a load for the grid, and a discharging EV is a power source for the grid when EVs are connected to a distribution power network. Due

to the onboard batteries energy storage technology, the vehicle-to-grid (V2G) technique can be utilized as a distributed energy storage unit. Therefore, EV can be a good solution for stabilizing isolated micro-gids. However, the major issue associated with isolated micro-grid is large frequency fluctuation due to intermittent renewable source connections where the load frequency control capability is not good enough to compensate for the unbalanced generation and the load demand. Load frequency control of the power system, also known as automatic generation control (AGC), is crucial. An AGC, a feedback control system, keeps a generator's output power at a predetermined frequency. One of AGC's goals is to keep the system frequency at a desired level and to preserve the power system's steady state performance [5].

It is common practice to utilize an artificial bee colony (ABC) for load frequency control (LFC) in linked power systems with one, two, or more zones [6]. Additionally, frequency and reactive power regulation is the main function of the LFC loop. The main goal of this effort is to stop all of the system's oscillations caused by the unsettling influence and restore frequency at a feignedly reasonable cost.

Researchers in [6] developed a single-area power system that also used the root locus technique to evaluate the performance of the fractional order PID (FOPID) controller to that of the PID controller. The research then expands to include a three- or multi-area thermal power system with a nonlinear generation rate constraint (GRC). A FOPID controller is employed to enhance the system's dynamic response, and the enhanced values are tuned using the bacterial foraging optimization algorithm (BFOA), which uses the integral time multiplied by absolute error as an objective function. Finally, including transport delay (TD) allows for investigating how resilient the proposed controller is. However, sending the control signal from the control center is not considered, leading to a longer settling time. However, the authors [7] noted that a power system's nonlinear load frequency controller was optimized using a novel artificial intelligent search technique that considered PID. A PID controller is included with a two-area non-reheat thermal system. The methodology employed is called the differential evolution technique. BFOA is used to find the best controller settings to minimize the time domain objective function. However, since the environment is unknown, the strategies struggle with robustness. The study [8], suggests a better particle swarm optimization approach to improve electric vehicle charging models. It illustrates how an orderly charging control technique can raise grid operation's effectiveness, security, and dependability. In order to optimize the electric vehicle charging model, the study considers various limitations and optimization targets, including load variance, load peak-valley difference, and charging cost. Additional study is required on energy storage systems with micro-grid support capabilities and charging methods for electric vehicles based on renewable energy sources. Moreover, in [9], the study emphasized the benefits of high-frequency ac-link-based converters, which provide a decreased part count, size, and centralized control, contributing to better efficiency and compactness. It also supports the creation of multiport converters that are optimized and more effective for combining energy storage and renewable energy sources. But the study might be restricted in its use to ac grids alone.

Community micro-grids (CMG) modelling and frequency management under stochastic solar and wind sources to account for the impact of modelling ambiguity. The mathematical modelling features of various CMG sources and the community microgrid model's robust control design. A resilient design using a fixed structure high infinite (H) synthesis approach was provided. It is suggested that a robust controller architecture for CMG be used to manage stochastic input disturbances, including abrupt changes in power from solar and wind sources and the model uncertainty that causes parametric perturbations. Using a more powerful controller than the PID controller, a reduction of 30% in frequency overshoot and settling time is made. Nevertheless, the rise or fall of disturbances like wind and solar also affects how far the frequency deviation overshoots its peak value. The difference in the rate of rising or dropping thereby introduces oscillations in the frequency of CMG's suggested controller, resulting in long settling times [10].

Improvements need to be made to specific conditions, a challenge must be overcome, or a problematic topic has been raised in the research literature about load frequency regulation. Numerous controllers are employed in searching for reliable frequency control to maintain the power system's frequency working regularly. The majority of load frequency controllers are proportional-integral (PI) controllers, which have a constrained amount of programmable time [11]–[13]. Furthermore, when a proper optimization technique is not used and due to the additional parameters compared to traditional PID parameters, the optimum FOPID parameters are more time-consuming and labor-intensive to achieve [14]. If a proper objective function is not employed to explore the controller gains, the controller gains are at a level that strikes a balance between quick transient recovery and low undershoot in the dynamic response of the entire system. These control systems were generally limited in producing deep undershoots and long settling times. In order to achieve a micro-grid system with a reliable load frequency management scheme, reduced undershoots, and settling time utilizing fractional order PID controller tuned with grasshopper optimization algorithm (GOA), it is important to address the concerns identified.

Researchers often use fractional order (FO) controllers to tackle engineering challenges due to their adaptability and elevated degree of freedom. However, in most cases, adding hyper-damped poles increases

the need for tuning, and the stability scale has been increased [15]. Therefore, an attempt is made to solve LFC challenges using a modified FOPID with EV and renewable energy sources, as no attempt has been made in the literature.

This study focuses on designing a microgrid frequency oscillation damping controller with a modified fractional-order proportional-integral-differential (MFOPID) controller based on an electric vehicle (EV) and renewable energy source using GOA to turn the controller parameters. The MFPOID controller is used to improve the dynamic response of the conventional energy sources (wind, solar) and EV with a metaheuristic approach called GOA to fine-tune the controller gains of MFOPID. Therefore, the contributions of the study are: i) The best MFOPID controller parameters are found using a metaheuristic optimization method (GOA), which also controls the frequency and frequency deviation of the system; ii) The proposed model took into account EVs and renewable energy sources; and iii) Evaluation of the performance of the modified FOPID controller and the conventional FOPID controller to validate and establish superiority.

2. METHOD

2.1. Proposed microgrid system model

The general schematic diagram of the proposed model with various energy sources is shown in Figure 1. This is made up of a DEG, model for solar PV, wind turbine, ultracapacitor and lumped electric vehicle (EV) model. The overall power generation is determined by: i) diesel generator output power, ii) the lumped electric vehicle output power, iii) the ultra-capacitor exchange power, iv) wind turbine generator output power, and v) the solar photovoltaic output power.
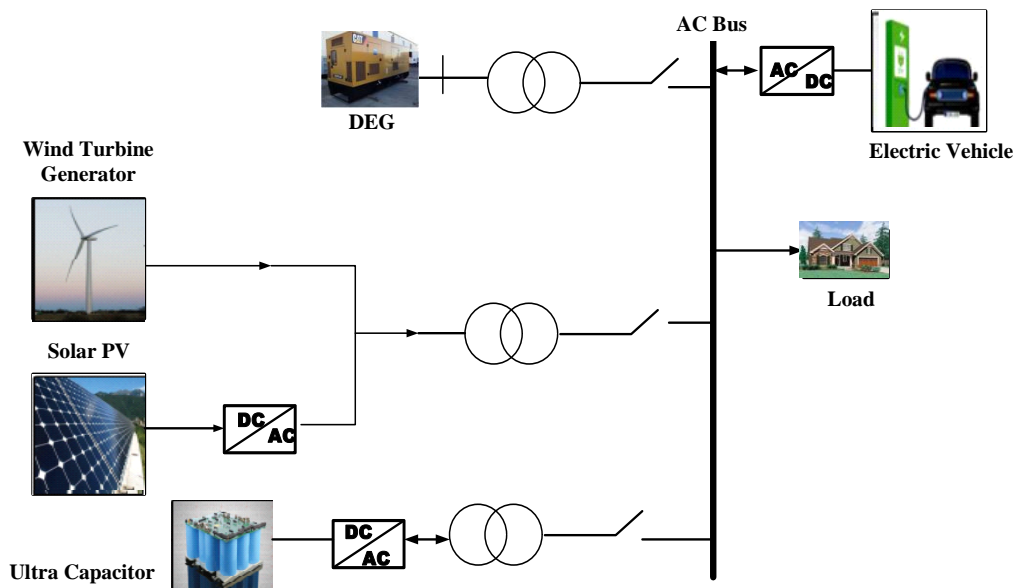

Figure 1. Overall schematic diagram of the proposed model

2.2. Diesel generator model

In the diesel generator model, the speed governor can effectively overturn a small range of frequency deviations caused by disturbances that affect the power system network; however, the primary frequency control cannot completely eliminate bigger disturbances to a state of zero deviation. In this situation, the secondary load frequency control is vital to alter the speed governor's characteristics and eventually bring the frequency variation to zero [16].

The diesel generator adjusts for the necessary power in the microgrid using the governor, turbine, and speed regulator.

$$G_{DS}(s) = \frac{-1}{R}\left(\frac{1}{1+sT_g} \times \frac{1}{1+sT_t}\right) \tag{1}$$

Where R is the regulator speed, T_g is the time constant of the governor and T_t is the time constant of turbine. Figure 2 represents the overall transfer function, where ΔP is the input reference power and ΔP_{DG} is the DG output power.

2.3. Wind turbine model

The wind's kinetic energy is transformed into electrical energy in wind turbines by passing the energy to the rotor, which then generates electricity. The system comprises a generator coupled to a shaft that transforms the rotor's rotation into electrical energy. Due to its high efficiency, low maintenance cost, easy controllability, and high power density, the variable speed direct drive permanent magnet synchronous generator (PMSG) is now widely employed in wind power systems [17]. However, the generator model is analyzed using the d – q reference frame and its voltage equation is given as (2) and (3).

$$V_d = -R_S i_d - L_d \frac{di_d}{dt} + \omega_r L_q i_q \tag{2}$$

$$V_q = -R_S i_q - L_q \frac{di_q}{dt} - \omega_r L_d i_d + \omega_r \lambda_m \tag{3}$$

The electromagnetic torque is expressed as (4).

$$T_e = \frac{1}{2} p \left[\lambda i_q + \left(L_d - L_q \right) i_d i_q \right] \tag{4}$$

Where; L_q and L_d are q- and d-axis inductance respectively, i_q and i_d are q-and d-axis current, V_q and V_d are q- and d-axis voltage, ω_r is rotor angular velocity, λ_m induced flux, and p is the pole pairs number.

The power generation from the wind generator depends on the wind speed, which is stochastic. The expression represent the wind turbine power output [18], [19].

$$P_{WT} = \frac{1}{2} \rho \Lambda C_p V_W^3 \tag{5}$$

Where ρ the density of the air, Λ swept area of the blade, V_W speed of the wind, C_ρ and the power coefficient. The wind turbine transfer function is given by ignoring all non-linearity and is as (6),

$$G_{WTG}(s) = \frac{\Delta P_{WTG}}{\Delta P_{WT}} = \frac{k_{wtg}}{1+sT_{wtg}} \tag{6}$$

Where ΔP_{WTG} is the turbine power generation deviation, ΔP_{WT} is the deviation in wind power available, ΔK_{wtg} is the change in gain constant and T_{wtg} time constant, and (6) can be represented as in Figure 3.
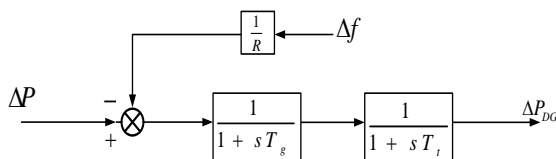

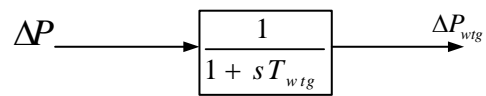Figure 2. Diesel generator transfer function block   Figure 3. Block diagram of wind turbine generator

2.4. Solar PV model

The difference between the diode current and the photogenerated current can be used to illustrate how a cell behaves when acting as a current generator [20]. The equivalent circuit model ideal PV is in Figure 4.

$$I_{ph} = I_{pv} + I_D \tag{7}$$

The (8) provides a current to the diode [20], [21]:

$$I_D = I_o (\ell^{\frac{qV_D}{KT}} - 1) \tag{8}$$

Where I_o is the current in dark saturation I_D is the diode net current, V_D is the supply voltage to the diode, q is the electron charge, K is Boltzmann's constant and T is the absolute temperature. By substituting (8) into (7).

$$I_{ph} = I_{pv} + I_D = I_{PV} + I_o(\ell^{\frac{qV_D}{KT}} - 1) \tag{9}$$

Add (6) into (9) to obtain (10).

$$I_{ph} = \frac{V_D - V_{PV}}{R} + I_o(\ell^{\frac{qV_D}{KT}} - 1) \tag{10}$$

The PV power output ΔP_{PV} is determined by (11).

$$\Delta P_{PV} = V_{PV} I_{PV} \tag{11}$$

Considering linear relationship between power deviation and time constant T_{PV}.

$$\Delta P = \Delta P_{pv}(1 + sT_{PV}) \tag{12}$$

Figure 5 shows PV transfer function block. The overall PV transfer function is provided by (13).

$$G(s) = \frac{\Delta P_{pv}}{\Delta P} = \frac{1}{(1 + sT_{PV})} \tag{13}$$
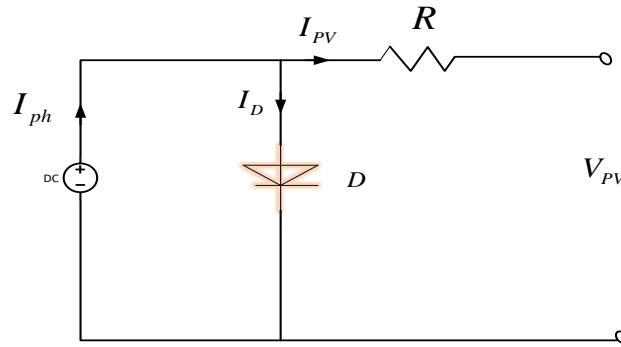
Figure 4. PV equivalent circuit

2.5. Ultra capacitor model

This electric double-layer capacitor or ultra capacitor (UC) is used for energy storage in renewable energy sources, hybrid and electric vehicles, and biomedical sensors. The UC is connected to the ac bus via an inverter (DC-AC), providing bidirectional power to the bus bar [22]. If the power generated is more than the required power, the UC will operate in charging mode. Otherwise, the ultracapacitor will be working in discharging mode. It plays a significant role by increasing the system inertia via power absorption or injection. The transfer function of ultra-capacitor taken into account of fractional calculus [23] is given as (14):

$$G_{UC}(s) = k_{UC}\left(1 + \frac{1}{s^\beta T_{UC}}\right) \tag{14}$$

Where T_{UC} is the time constant for the fractional order model of UC, and s^β is the system frequency domain. The entire system is represented mathematically with the defined terms in this section, as shown in Figure 6 and (15). Transfer function gives as (15).

$$G_{uc}(s) = \frac{1}{(1 + sT_{uc})} \tag{15}$$

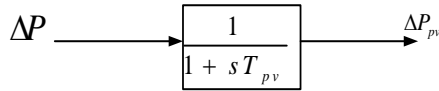Where T_{uc} is the time constant for UC.
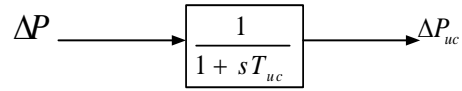
Figure 5. Block diagram of the photovoltaic

Figure 6. Block diagram of ultracapacitor

2.6. Electric vehicle model

This study focuses on EVs' role in an island microgrid's frequency control system using V2G inclusion. The system block diagram shows the model of the transfer function of EV is presented in Figure 7. In the EV model, the transfer function for calculating the time delay is represented by a first-order transfer function with time delay T_{EV} [24].

$$G_{EV}(s) = \frac{\Delta P_{EV}(s)}{\Delta P_E(s)} = \frac{K_{Ev}}{1+sT_{EV}} \tag{16}$$
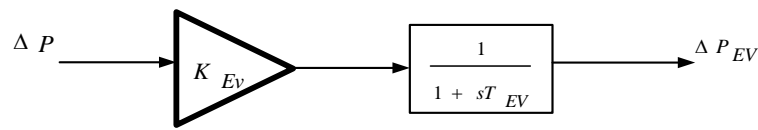
Figure 7. Block model of EV

2.7. Load model

The frequency of the system is affected by changes in load. The following expression represents the transfer function for the change as (17).

$$G_L = \frac{1}{1+sM} \tag{17}$$

Where $M = 2H$ and H is the inertia of the load. The net power generated based on supply load is given by (18) [25].

$$P_{Load} = P_{DG} + P_{WTG} + P_{PV} \pm P_{EV} \pm P_{UC} \tag{18}$$

In order to stabilized demand and supply units when a step load is applied, renewable energy sources like PV, WTG, and energy storage systems all generate power.

$$\Delta P_{Load} + \Delta P_{DG} + \Delta P_{WTG} + \Delta P_{PV} + \Delta P_{EV} + \Delta P_{UC} = 0 \tag{19}$$

Power and frequency are represented as (20).

$$\Delta f = \frac{1}{2H+D}(\Delta P_{DG} + \Delta P_{WTG} + \Delta P_{PV} + \Delta P_{EV} + \Delta P_{UC} - \Delta P_{Load}) \tag{20}$$

The general schematic diagram of the microgrid transfer function is formed using the summation point to combine them, as shown in Figure 8, having obtained the transfer function of each energy source. The net power generation of the system is determined by the following: a) solar output power (Ppv), b) wind generator power, c) diesel generator output power, d) ultracapacitor exchange power, and e) the V2G output power.

2.8. Grasshopper optimization algorithm

The grasshopper optimization algorithm (GOA) is an anatomical optimization technique based on the mathematical modelling of nature. Considering its ability to deliver and its robustness in locating the best solution, an approximation optimal solution close to a global minimum, it is frequently utilized to tackle optimization problems in several application domains. The behavior of grasshopper swarms is mathematically described in (21).

$$P_i = S_i + G_i + A_i \tag{21}$$

Where Pi represents the ith grasshopper's position, S_i represents grasshopper's social interaction, G_i represents the ith grasshopper's gravitational pull, and A_i represents wind advection:

$$C = C_{max} - t \frac{C_{max} - C_{min}}{t_{max}} \tag{22}$$

and C stands for the variable in the optimization algorithm, C_{max} and C_{min} are its maximum and minimum values, respectively, t stands for the iteration currently being performed, and t_{max} is its maximum number. The (22) can be changed as follows to achieve a random behavior of grasshoppers as in (23):

$$P_i = r_1 S_i + r_2 G_i + r_3 A_i \tag{23}$$

where r_1, r_2, and r_3 are all arbitrary numbers between 0 and 1, respectively.
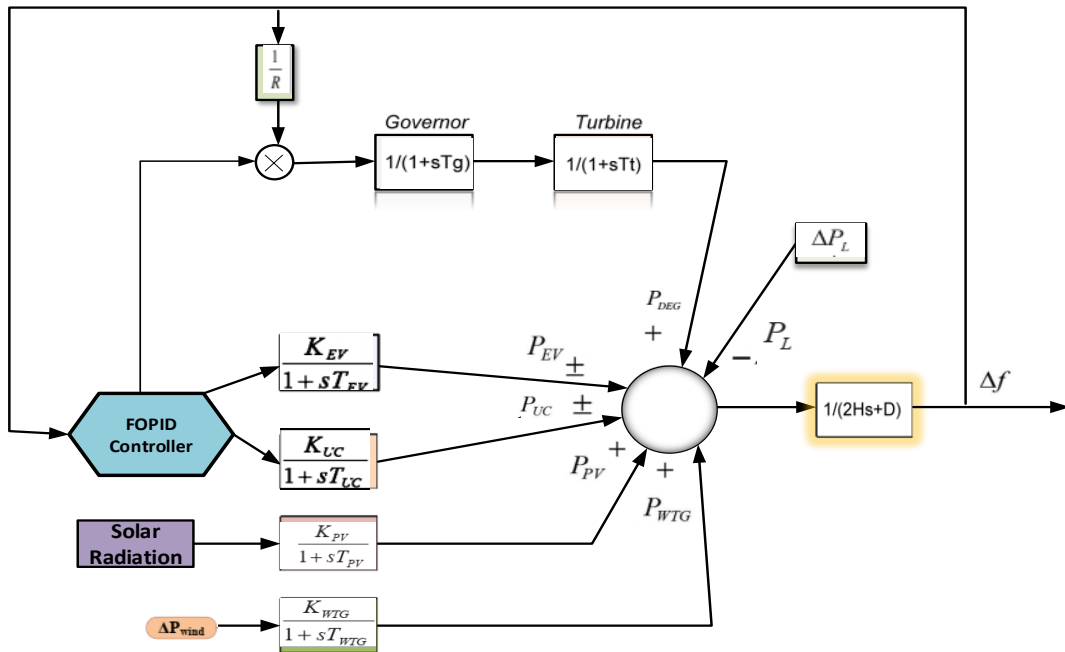
Figure 8. Schematic diagram of the proposed LFC model

− Fitness function and MFOPID structure

The standalone microgrid's frequency deviation is considered a reference for the optimal tuning of the PID and MFOPID gains. Therefore, the dynamic performance of the proposed controller is investigated by the integral time absolute error (ITAE) method. The advantages of ITAE over other performance index criteria integral square error (ISE) and integral absolute error (IAE) are smaller overshoot/undershoot and reduced oscillation.

The integral term (Ki) in the MFOPID controller is feedforward with the integrator order (l), while the other parameters are feedback, whereas all gains in the FOPID controller are feedforward. The MFOPID and FOPID controller output is given in (24) and (25), respectively, as a differential equation.

$$u(t) = e(t)D^{-\lambda}k_i - y(t)\left[k_p + D^{\mu}k_d\right] \tag{24}$$

$$u(t) = e(t)K_p + e(t)D^{-\lambda}k_i + e(t)D^{\mu}k_d \tag{25}$$

Taking the Laplace transform of (25) and (26), the transfer function of the control loops corresponding to MFOPID and FOPID is given as (26) and (27).

$$G_{MFOPID}(s) = \frac{G_p(s)k_i}{s^{\lambda} + s^{\lambda}k_p + G_p(s)k_i + k_d s^{\lambda}s^{\mu}} \tag{26}$$

$$G_{FOPID}(s) = \frac{[s^\lambda k_p + k_d s^\lambda s^\mu + k_i] G_p(s)}{s^\lambda + [s^\lambda k_p + k_d s^\lambda s^\mu + k_i] G_p(s)} \tag{27}$$

The proposed MFOPID controller overcomes these effects of zeros as in (26), enhancing the system response by switching the Kp and Kd gains from the traditional FOPID controller's forward direction to its feedback path. The MFOPID controller's block diagram is shown in Figure 9(a) while the block diagram of the conventional FOPID is presented in Figure 9(b). The system response is better than the system response of the FOPID controller, as shown in the model equations because it is difficult to change the system's response when FOPID has two zeros, which has the effect of either a more extreme overshoot or a quicker rise to the peak value.
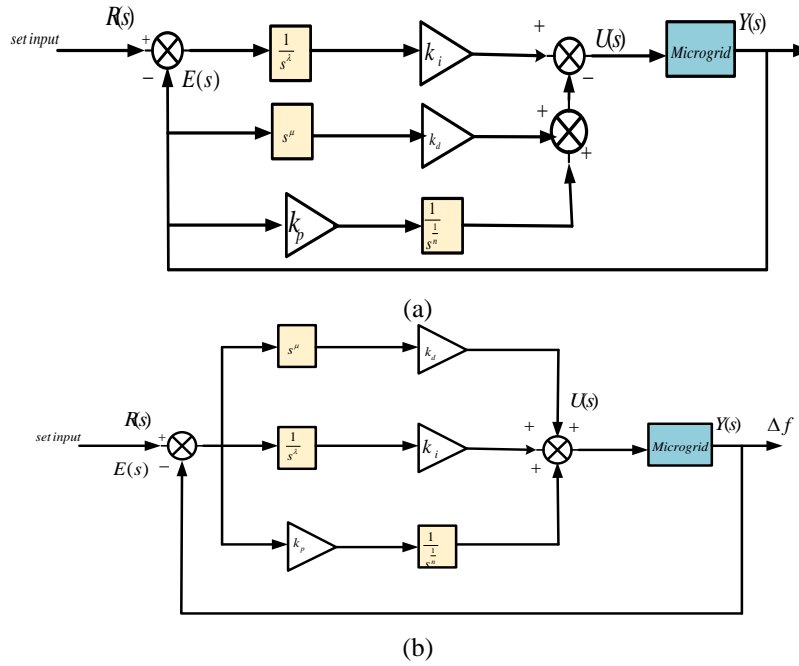
Figure 9. Design of the controller structure used in the MG: (a) MFOPID controller and
(b) FOPID controller

The desired objective function is the cost function of ITAE is given as (28).

$$J_{objective} = min\,i\,mize(ITAE) \tag{28}$$

Subject to (29)-(31).

$$k_p^{Min} \le k_p \le k_p^{Max}, k_d^{Min} \le k_d \le k_d^{Max}, k_i^{Min} \le k_i \le k_i^{Max}, \lambda^{Min} \le \lambda \le \lambda^{Max}, \mu^{Min} \le \mu \le \mu^{Max} \tag{29}$$

$$ITAE = \int_0^{t_s} t|u(t)|dt \tag{30}$$

$$J_{objective} = min\left(\int_0^{t_s} t[|u(t)|]\,dt\right) \tag{31}$$

Substituting $u(t)$ from (26) and (27) into (31) to obtain:

$$J_{objective} = min\left(\int_0^{t_s} t[|e(t)D^{-\lambda}k_i - y(t)[k_p + D^\mu k_d]|]\,dt\right) \tag{32}$$

$$J_{objective} = min\left(\int_0^{t_s} t[|e(t)K_p + e(t)D^{-\lambda}k_i + e(t)D^\mu k_d|]\,dt\right) \tag{33}$$

Where K_P, K_i and K_d stand for proportional, integral and differential gains, respectively, and μ and λ, are the fractional powers of the differentiator and integrator, respectively. For the best tuning of the MFOPID gain, the frequency deviation of the standalone microgrid and the overall transfer function in Figure 8 are used as references.

3.   RESULTS AND DISCUSSION

The optimal parameters for each population size are shown in Table 1 of the MFOPID, with the best fitness score for the different search agents. The obtained result based on minimizing the objective function, ITAE, with five, ten, fifteen, and twenty search agents are used (GOA) for 50 iterations to determine the most suitable parameters gain of the controller are 175.2614, 35.072, 32.2914, and 59.6325, respectively and the corresponding plots are presented in Figure 10. Also shown in Table 1 are the relevant MFOPID parameter values that were acquired. In Figure 11, the ITAE with a population size of fifteen and objective function of 32.2914 is the minimum value among all the different population sizes and thus has the best fitness score. The parameter's value of the MFOPID is therefore applied to obtain the desired result of the load frequency control of the microgrid using the MFOPID controller tuned with GOA.
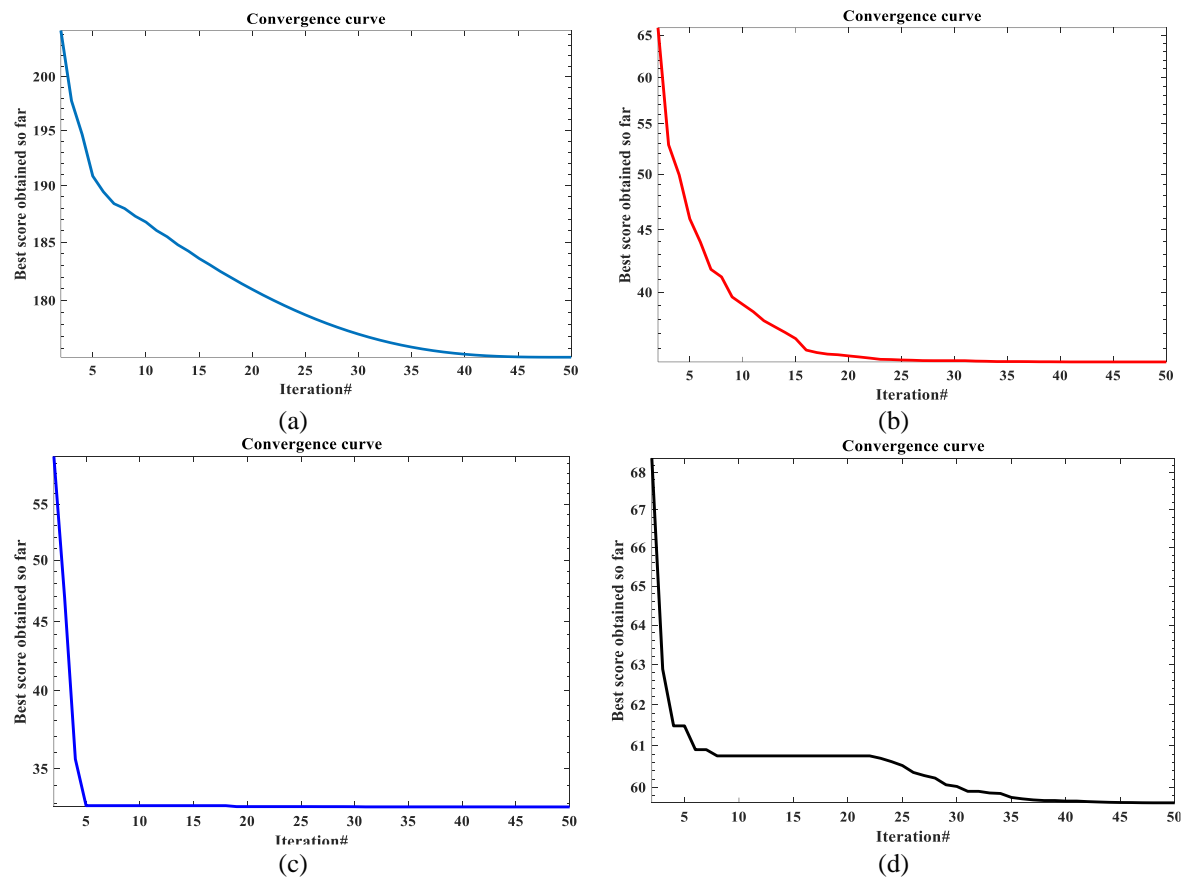

Figure 10. Comparing the best fitness with different population size: (a) population size of 5, (b) population size of 10, (c) population size of 15, and (d) population size of 20

Table 1. Optimal parameters for different population sizes

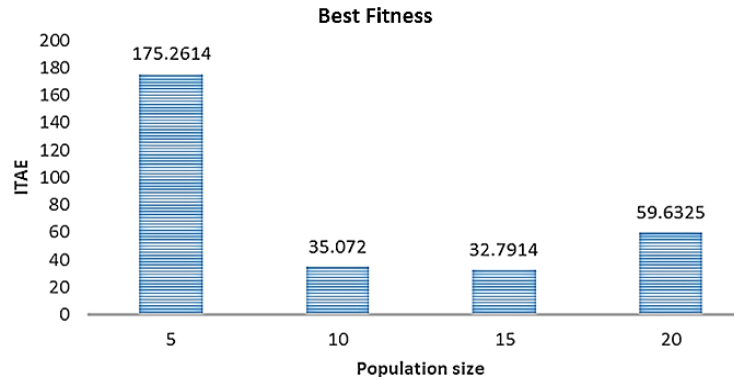| Population size	Best Fitness Score	Kp	Ki	lambda	Kd	Mu
5	175.2614	6.04074	12.5647	0.0549967	2.54743	0.480602
10	35.072	1.35805	16	0.0551203	1.43335	0.22323
15	32.2914	1.349	16	0.056761	2.64897	0.209883
20	59.6325	1.88225	15.9999	0.0482958	4.50873	0.339338

Figure 11. ITAE for each population size

The results that compared the proposed controller MFOPID and FOPID without optimization are presented in Figure 12, and the frequency deviation is 30.4432 Hz and 35.8206 Hz for MFPOID and FOPID, respectively, with the lowest frequency from MFOPID. The simulation results obtained for the proposed model and FOPID optimized with GOA are shown in Figure 13. The settling time is analyzed, which is the time required for the damped oscillation to reach and stay within the specified range of (2% to 5%) of its final value. It takes 6.9068 sec of the proposed model to settle compared to 16.6796 sec of FOPID. This provides important information related to the speed and quality of the response generated on the microgrid. The system performance frequency is presented with an undershoot of 19.485 Hz and 14.1151 Hz for MFOPID and FOPID, respectively.
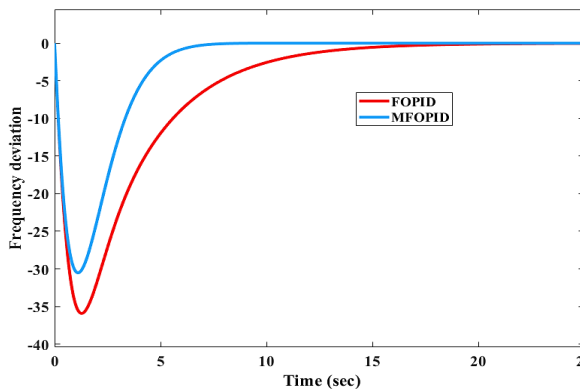
Figure 12. System's frequency deviation in Hz with MFOPID and FOPID
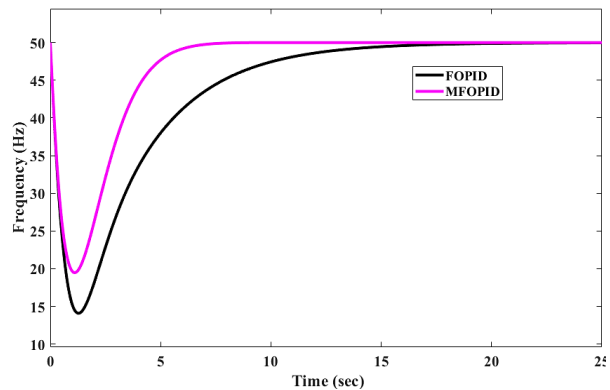
Figure 13. System's frequency control performance in Hz with MFOPID and FOPID controller

4. CONCLUSION

Weather-dependent renewable energy sources, V2G electric vehicles, and quick load changes cause microgrid frequency variations. The resilient load frequency controller reduces frequency variation to reduce frequency undershoot, duration to undershoot, settling time, and final settling zone. Thus, an MFOPID controller is developed for the microgrid LFC to tackle the energy source's intermittent and reduce the fast dynamic of response generated on the microgrid. Its performance is compared to traditional FOPID to determine its robustness and optimize using the GOA technique. Multiple search agent population sizes were tested to optimize and select the optimal gains parameters. MFOPID outperformed FOPID.

The proposed MFOPID with GOA improved system performance frequency by 19.485 Hz compared to 14.1151 Hz of the benchmark model. and it takes 6.9068 sec of the proposed model to settle compared to 16.6796 sec of FOPID. The population size of the optimization technique does not influence the minimized objective function (best fitness score) for the optimal MFOPID parameters changed by GOA, regardless of the number of search agents. This analysis found that 15-search agent populations had the lowest objective function.

REFERENCES

[1]   F. Gonzalez Venegas, M. Petit, and Y. Perez, "Active integration of electric vehicles into distribution grids: Barriers and frameworks for flexibility services," *Renewable and Sustainable Energy Reviews*, vol. 145, 2021, doi: 10.1016/j.rser.2021.111060.

[2]   W. Tong, A. Hussain, W. X. Bo, and S. Maharjan, "Artificial Intelligence for Vehicle-To-Everything: A Survey," *IEEE Access*, vol. 7, pp. 10823–10843, 2019, doi: 10.1109/ACCESS.2019.2891073.

[3]   M. Abdillah, R. H. Pratama, N. I. Pertiwi, and H. Setiadi, "Retired electric vehicle battery to reduce the load frequency control oscillation in the micro grid system," *Indonesian Journal of Electrical Engineering and Computer Science*, vol. 28, no. 3, pp. 1266–1275, 2022, doi: 10.11591/ijeecs.v28.i3.pp1266-1275.

[4]   M. S. Hossain, L. Kumar, M. El Haj Assad, and R. Alayi, "Advancements and Future Prospects of Electric Vehicle Technologies: A Comprehensive Review," *Complexity*, vol. 2022, 2022, doi: 10.1155/2022/3304796.

[5]   A. Dubey and P. Bondriya, "Literature Survey on Load Frequency Controller," *International Research Journal of Engineering and Technology*, 2016, [Online]. Available: www.irjet.net.

[6]   N. E. Y. Kouba, M. Menaa, M. Hasni, and M. Boudour, "Optimal load frequency control based on artificial bee colony optimization applied to single, two and multi-area interconnected power systems," *3rd International Conference on Control, Engineering and Information Technology, CEIT 2015*, 2015, doi: 10.1109/CEIT.2015.7233027.

[7]   E. S. Ali and S. M. Abd-Elazim, "BFOA based design of PID controller for two area Load Frequency Control with nonlinearities," *International Journal of Electrical Power and Energy Systems*, vol. 51, pp. 224–231, 2013, doi: 10.1016/j.ijepes.2013.02.030.

[8]   A. Rabie, A. Ghanem, S. S. Kaddah, and M. M. El-Saadawi, "Electric vehicles based electric power grid support: a review," *International Journal of Power Electronics and Drive Systems*, vol. 14, no. 1, pp. 589–605, 2023, doi: 10.11591/ijpeds.v14.i1.pp589-605.

[9]   S. Arulmozhi and K. R. Santha, "Review of multiport isolated bidirectional converter interfacing renewable and energy storage systems," *International Journal of Power Electronics and Drive Systems*, vol. 11, no. 1, pp. 466–476, 2020, doi: 10.11591/ijpeds.v11.i1.pp466-467.

[10] D. Kumar, H. D. Mathur, S. Bhanot, and R. C. Bansal, "Modeling and frequency control of community micro-grids under stochastic solar and wind sources," *Engineering Science and Technology, an International Journal*, vol. 23, no. 5, pp. 1084–1099, 2020, doi: 10.1016/j.jestch.2020.02.005.

[11] Y. V. Hote and S. Jain, "PID controller design for load frequency control: Past, Present and future challenges," *IFAC-PapersOnLine*, vol. 51, no. 4, pp. 604–609, 2018, doi: 10.1016/j.ifacol.2018.06.162.

[12] S. K. Aditya and D. Das, "Design of load frequency controllers using genetic algorithm for two area interconnected hydro power system," *Electric Power Components and Systems*, vol. 31, no. 1, pp. 81–94, 2003, doi: 10.1080/15325000390112071.

[13] M. Almaged, S. I. Khather, and A. I. Abdulla, "Design of a discrete PID controller based on identification data for a simscape buck boost converter model," *International Journal of Power Electronics and Drive Systems*, vol. 10, no. 4, pp. 1797–1805, 2019, doi: 10.11591/ijpeds.v10.i4.pp1797-1805.

[14] F. A. Hasan and L. J. Rashad, "Fractional-order PID controller for permanent magnet DC motor based on PSO algorithm," *International Journal of Power Electronics and Drive Systems*, vol. 10, no. 4, pp. 1724–1733, 2019, doi: 10.11591/ijpeds.v10.i4.pp1724-1733.

[15] C. Michael, O. J. Tola, M. N. Nwohu, and J. G. Ambafi, "Load Frequency Control of a Microgrid using Fractional Order PID Controller," *Proceedings of the 2022 IEEE Nigeria 4th International Conference on Disruptive Technologies for Sustainable Development, NIGERCON 2022*, 2022, doi: 10.1109/NIGERCON54645.2022.9803186.

[16] C. Shah, R. W. Wies, T. M. Hansen, R. Tonkoski, M. Shirazi, and P. Cicilio, "High-Fidelity Model of Stand-Alone Diesel Electric Generator With Hybrid Turbine-Governor Configuration for Microgrid Studies," *IEEE Access*, vol. 10, pp. 110537–110547, 2022, doi: 10.1109/ACCESS.2022.3211300.

[17] O. J. Tola, E. A. Umoh, E. A. Yahaya, and O. E. Olusegun, "Permanent Magnet Synchronous Generator Connected to a Grid via a High Speed Sliding Mode Control," *International Journal of Robotics and Control Systems*, vol. 2, no. 2, pp. 379–395, 2022, doi: 10.31763/ijrcs.v2i2.701.

[18] F. E. Blouh, B. Boujoudi, and M. Bezza, "Wind energy conversion system based on DFIG using three-phase AC-AC matrix converter," *International Journal of Power Electronics and Drive Systems*, vol. 14, no. 3, pp. 1865–1875, 2023, doi: 10.11591/ijpeds.v14.i3.pp1865-1875.

[19] Y. Charabi and S. Abdul-Wahab, "Wind turbine performance analysis for energy cost minimization," *Renewables: Wind, Water, and Solar*, vol. 7, no. 1, 2020, doi: 10.1186/s40807-020-00062-7.

[20] M. Asim, A. Sarwar, M. Shahabuddin, and M. S. Manzar, "Development of solar photovoltaic model for wide range of operating conditions," *International Journal of Power Electronics and Drive Systems*, vol. 12, no. 4, pp. 2483–2491, 2021, doi: 10.11591/ijpeds.v12.i4.pp2483-2491.

[21] H. Attia and K. Hossin, "Hybrid technique for an efficient PV system through intelligent MPPT and water cooling process," *International Journal of Power Electronics and Drive Systems*, vol. 11, no. 4, pp. 1835–1843, 2020, doi: 10.11591/ijpeds.v11.i4.pp1835-1843.

[22] R. Moualek, N. Benamrouche, N. Benyahia, and A. Bousbaine, "Hybrid multi power sources PEMFC/battery/supercapacitor real time setup energy conversion system," *International Journal of Power Electronics and Drive Systems*, vol. 14, no. 3, pp. 1844–1854, 2023, doi: 10.11591/ijpeds.v14.i3.pp1844-1854.

[23] R. Kopka and W. Tarczyński, "A fractional model of supercapacitors for use in energy storage systems of next-generation shipboard electrical networks," vol. 4177, no. November, 2017, doi: 10.1080/20464177.2017.1386818.

[24] H. Abubakr, A. Lashab, J. C. Vasquez, T. H. Mohamed, and J. M. Guerrero, "Novel V2G regulation scheme using Dual-PSS for PV islanded microgrid," *Applied Energy*, vol. 340, 2023, doi: 10.1016/j.apenergy.2023.121012.

[25] D. Kumar, H. D. Mathur, S. Bhanot, and R. C. Bansal, "Frequency regulation in islanded microgrid considering stochastic model of wind and PV," *International Transactions on Electrical Energy Systems*, vol. 29, no. 9, Sep. 2019, doi: 10.1002/2050-7038.12049.

BIOGRAPHIES OF AUTHORS

Omokhafe James Tola was born in Ososo Edo state, Nigeria. He received his degree in Electrical and Computer Engineering from Federal University of Technology Minna, Nigeria, in 2004, and M.Eng. degree in Electrical Power and Machines from Federal University of Technology Minna in 2012 and Ph.D. degree in Electrical Machines and Drive from University of Nigeria Nsukka, Nigeria in 2019. His research interests include; power electronics and drive and power systems control and dynamics, modeling of electrical machines, hybrid renewable energy systems. He can be contacted at email: omokhafe@futminna.edu.ng.

Ovis Daniel Irefu obtained his bachelor's degree in Electrical and Computer Engineering from the Federal University of Technology Minna, Nigeria in 2014 and an M.Sc. in Electrical and Electronic Engineering at the University of Benin, Nigeria in 2019. He is currently a Ph.D. student at the Department of Electrical Engineering, UNT College of Engineering, University of North Texas, Discovery Park Denton, Texas USA. He can be contacted at email: ovisirefu@my.unt.edu.

James Garba Ambafi Obtained BEng in Electrical and Electronics Engineering from the Federal University of Technology Yola, Nigeria, an MEng degree in Electrical Power and Machines from the Federal University of Technology Minna, Nigeria, and a Ph.D. degree in Electrical Engineering at Bayero University, Kano, Nigeria. He is currently a Senior Lecturer in the Department of Electrical & Electronics Engineering at the Federal University of Technology, Minna. Nigeria. His research interests include; power system stability and control, hybrid renewable energy systems. He can be contacted at email: ambafi@futminna.edu.ng.